An Interpolation-Based Solution to Use Low Sampling Rate Records in Traveling Wave-Based Fault Location Methods

E. P. A. Ribeiro, F. V. Lopes, K. M. Silva, A. G. Martins-Britto, Raphael L. A. Reis, Caio M. Moraes, Rodrigo L. Agostinho, Marco A. M. Rodrigues

***Abstract*—This paper presents an interpolation-based solution that allows the application of traveling wave (TW)-based algorithms even using sampling rates lower than those typically considered as a requirement for classical approaches. Two phasor (PH)-based and one TW-based fault location methods are compared with the proposed technique and applied through Alternative Transients Program (ATP) fault simulations in a 500 kV/60 Hz Brazilian double circuit series-compensated transmission lines with high-voltage direct current lines (HVDCs) and static var compensators (SVCs) in the vicinity. The results show that the proposed interpolation-based technique is reliable and suitable for TW-based fault location using data records with sampling rates lower than those used in commercially available equipment. Moreover, its accuracy is comparable to classical TW-based fault location solutions, revealing its usefulness for practical application when only traditional digital fault recorders (DFRs) are available.**

***Keywords*—Traveling waves, fault location, interpolation, power systems, transmission line, sampling rate.**

I. Introduction

FAULT location methods play an essential role in power system operation and maintenance procedures. In high, extra-high, and ultra-high voltage transmission lines, the reliability and accuracy of fault location estimations can be crucial to speed up the power supply restoration. It is further important in cases of huge overhead series-compensated lines installed on areas difficult to access by maintenance crews. In this context, technological advancements in power systems have led digital fault recorders (DFRs) and relays to incorporate high sampling rate A/D converters, leading the cost of some devices to increase. It reveals the need for reliable and low-cost fault location solutions, capable of providing accurate fault distance estimations, being immune to the complexity imposed by equipment installed in the vicinity for ensuring stability, and boosting transmission system efficiency, such as static var compensators (SVC), fixed series capacitors (FSC), and high-voltage direct current (HVDCs) lines [1]–[5].

In [1], a phasor (PH)-based transmission line fault location algorithm which use two-terminal data (i.e., it is double-ended) is presented. This method is called in this paper as PHFL and overcomes drawbacks of several fault location algorithms regarding transmission line asymmetry, charging effect, fault resistance, source impedance ratio, and poor response of capacitive voltage transformers. Nevertheless, it depends on the knowledge of accurate line parameters and precise voltage and current measurements from both line terminals.

In [2], four traveling wave (TW)-based fault location methods, called in this paper as TWFL, categorized into A, B, C, and D groups are assessed and suggested as a solution to overcome the well-known deficiencies of one and/or double-ended PHFL methods, such as high fault resistance values, infeed effect, series compensation, among others. The type A TWFL method uses one-terminal data (i.e., it is single-ended) and it assumes that the reflection coefficient at the fault point approximates $+1$, since the fault arc remains ionized for an extended period, presenting a very low fault resistance. Hence, the method depends on the detection of the first incident TW and first fault-reflected TW to estimate the fault location. On the other hand, the type D TWFL method is double-ended and it relies on detecting the first incident TWs at both monitored line terminals. Finally, methods of types B and C consist in active techniques, which require a pulse generating circuitry, being the type B-method double-ended and the type C-method single-ended. For both B and C methods, the injected pulses are provided by reclosing maneuvers of the faulty circuit at one terminal of the line, and by pulse-generating units, respectively.

In [6], one single-ended and one double-ended PHFL-based built into an actual commercial fault locator device are presented. Both methods are applied for unbalanced and three-phase faults using the negative-sequence and positive-sequence symmetrical components estimated from currents and voltages measured at both transmission line terminals. Indeed, despite the double-ended method presents a better accuracy than the single-ended one, it requires alignment between local and remote data, which can be achieved in the referred device by means of a point-to-point fiber optic channel. In counterpart, the single-ended method is affected by fault resistance, system non-homogeneity, and mutual coupling .

Eduardo P. A. Ribeiro, Kleber M. Silva, Amauri G. Martins-Britto, Caio Moraes are with University of Brasília (UnB), Brazil (email: {eduardopassos, klebermelo, amaurigm, caiomoraes}@lapse.unb.br).

F. V. Lopes and Raphael L. A. Reis are with Federal University of Paraíba (UFPB), Brazil (email: {felipelopes, raphael.leite}@cear.ufpb.br).

Rodrigo L. Agostinho is with Evoltz, Brazil (email: rodrigo.lehnemann@evoltz.com.br).

Marco A. M. Rodrigues is with CEPEL, Brazil (email: mamr@cepel.br).

This study was financed in part by the Coordenação de Aperfeiçoamento de Pessoal de Nível Superior - Brazil (CAPES) - Finance Code 001.

Paper submitted to the International Conference on Power Systems Transients (IPST2023) in Thessaloniki, Greece, June 12-15, 2023.

Finally, in [7], an assessment of the anti-aliasing filter influence on the classical type-D TWFL method described in [2] is investigated. As a result, it is identified that the frequency spectrum energy of line fault-induced transients is mainly concentrated at the lower band of the spectrum. Moreover, tests of disturbance detection were performed using the differentiator-smoother (DS) filter [4], also considering different numbers of DS coefficients (NDS). Thus, it was noticed that, if low anti-aliasing cutoff frequencies (fc) are used, i.e., if the lower part of the spectrum is considered, DS filters with large number of NDS can improve the TW amplitude estimation, also improving the TW detection.

Based on the above-mentioned considerations and taking into account findings reported in [7], an interpolation-based solution is proposed in this paper to allow the application of TW algorithms using relatively low frequency rates. Here, a sampling rate of 1,024 samples per cycle of 60 Hz (i.e., a sampling frequency of 61.44 kHz) is assessed. Such a sampling rate has been used in readily available DFRs [8], [9]. To evaluate the effectiveness of this proposal, the interpolation-based solution is applied to the type D TWFL method presented in [2], being compared with the traditional double-ended TWFL (i.e., with high sampling rates in the order of 1 MHz) and with two double-ended PHFL methods, which use a sampling frequency of 960 Hz, as reported in [1] and [6]. Such a comparison is carried out through simulations in a 500 kV/60 Hz Brazilian power system modeled in ATP/ATPDraw, which have SVCs, FSCs, and HVDCs in the near vicinity of the evaluated transmission line. The obtained results attest that the proposed solution is feasible, reliable, and accurate, providing fault distance estimations with accuracy comparable to those obtained using the classical TW-based methods which apply high sampling rates.

II. Description of Fault Location Methods

This section describes the theoretical background of the fault location methods analyzed in this paper. PHFL and TWFL techniques are explained and, for the sake of simplicity, they will be called hereafter PH1-method, PH2-method, and TW1-method.

A. PH1-Method

The PH1-method is the one reported in [1]. It assumes that, when a fault occurs, as depicted in Fig. 1, a relationship between the voltage at the fault point ($\hat{V}_F$) and the fault location (m) can be obtained in terms of voltages and currents measured at local terminal ($\hat{V}_L$ and $\hat{I}_L$) as follows:

$$\hat{V}_F = \cosh(\gamma \cdot m) \cdot \hat{V}_L - Z_c \cdot \sinh(\gamma \cdot m) \cdot \hat{I}_L \ , \quad (1)$$

or using the remote terminal data ($\hat{V}_R$ and $\hat{I}_R$):

$$\hat{V}_F = \cosh[\gamma \cdot (LL - m)] \cdot \hat{V}_R - Z_c \cdot \sinh[\gamma \cdot (LL - m)] \cdot \hat{I}_R \ , \quad (2)$$

where γ_x and Z_c are the line propagation constant and characteristic impedance, respectively [1].

Rearranging (1) and (2), m can be estimated by:

$$m = \text{Re}\left[\frac{\tanh^{-1}\left(-\frac{B}{A}\right)}{\gamma}\right] \ , \quad (3)$$

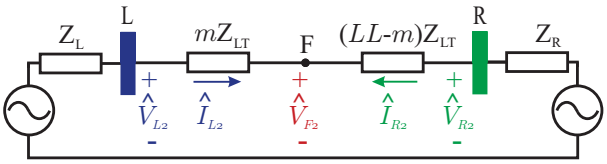

Fig. 1: Single-phase network.

being:

$$A = Z_C \cdot \cosh(\gamma \cdot LL) \cdot \hat{I}_R - \sinh(\gamma \cdot LL) \cdot \hat{V}_R + Z_C \cdot \hat{I}_L \ , \quad (4)$$

$$B = \cosh(\gamma \cdot LL) \cdot \hat{V}_R - Z_C \cdot \sinh(\gamma \cdot LL) \cdot \hat{I}_R - \hat{V}_L \ . \quad (5)$$

B. PH2-Method

The double-ended PH2-method is reported in [6]. It works based on the analysis of positive and negative-sequence voltage profiles along the line for both symmetrical and asymmetrical faults, respectively. From the negative-sequence network, as depicted in Fig. 2, the negative-sequence voltage at m ($\hat{V}_{F2}$) can be calculated considering measurements taken from both local and remote line terminals as:

$$\hat{V}_{F2} = \hat{V}_L - \frac{m}{LL} \cdot Z_2 \cdot \hat{I}_L \ , \quad (6)$$

$$\hat{V}_{F2} = \hat{V}_R - \frac{LL - m}{LL} \cdot Z_2 \cdot \hat{I}_R \ . \quad (7)$$

Rearranging (6) and (7), m can be obtained by:

$$m = LL \cdot \text{Re}\left[\frac{\left(\hat{V}_{L2} - \hat{V}_{R2}\right) + Z_2 \cdot \hat{I}_{R2}}{Z_2 \cdot \left(\hat{I}_{L2} - \hat{I}_{R2}\right)}\right] \ . \quad (8)$$

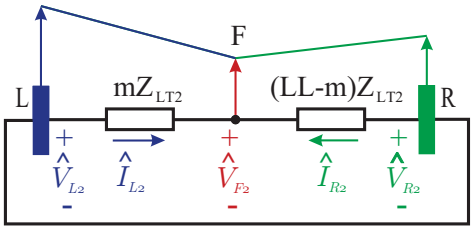

Fig. 2: Negative-sequence network.

C. TW1-Method

The traditional double-ended TWFL technique, reported in [2], is called here TW1-method. It is well-known that it depends on using sampling frequencies in the order of MHz to guarantee accurate fault distance estimations. Indeed, high sampling rates ensure high time resolutions, which in turn improve the accuracy of TW detectors. In internal fault cases, as depicted in Fig. 3, current TWs are launched toward both terminals, such that m can be estimated by (9), considering the transmission line travel time (τ) and the arrival time indexes of the first current TWs at both terminals (NL and NR for local and remote line ends, respectively).

$$m = \frac{LL}{2} \cdot \left[1 + \left(\frac{NL - NR}{\tau}\right)\right] \ . \quad (9)$$

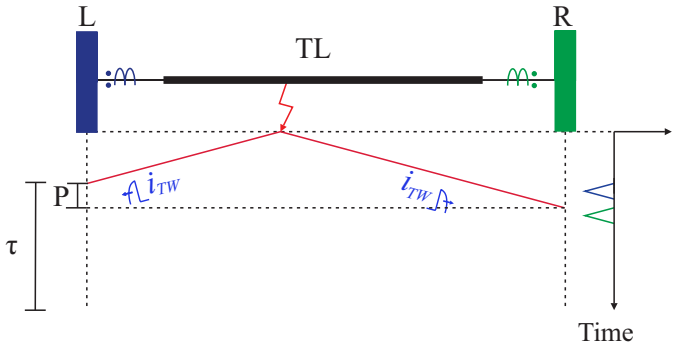

Fig. 3: Traveling waves internal faults pattern.

III. Linear Interpolation: Concept Review

Environments that incorporate the relationship between sampling rate and aliasing can make effective use of interpolation strategies for filtering implementation [10]. Notwithstanding, the interpolation procedure to increase the number of samples in a given record is called here upsampling [10], [11]. To explain such a procedure, consider a signal $x\,[n]$, whose number of samples will be increased by an integer factor L. Thus, analogously to a discrete-to-continuous conversion, if a continuous-time signal $x_c\,(t)$ is taken into account, the main objective of the interpolation is to obtain samples $x_i\,[n] = x_c\,(nTi)$, where $Ti = {}^{T}/_{L}$, from the sequence of samples $x\,[n] = x_c\,(nT)$, being T the time period of the analyzed signal. Therefore, one may observe that:

$$x_i\,[n] = x\,[{}^{n}/_{L}] = x_c\,(n \cdot {}^{T}/_{L})\,,\ n = 0, \pm L, \pm 2 \cdot L, \ldots\ , \quad (10)$$

where $x_i\,[n]$ can be obtained from $x\,[n]$ using discrete-time processing. The interpolation procedure occurs in two steps, as described in Fig. 4, where a sampling rate expander is computed via (11), being followed by a low-pass discrete-time filter with cutoff frequency ${}^{\pi}/_{L}$, gain L, and impulse response as represented in (12) [10].

$$x_e\,[n] = \sum_{k=-\infty}^{\infty} x\,[k] \cdot \delta\,[n - k \cdot L]\ . \quad (11)$$

$$h_i\,[n] = \frac{\sin\,({}^{\pi \cdot n}/_{L})}{{}^{\pi \cdot n}/_{L}}\ . \quad (12)$$

Therefore, according to [10], the linear interpolation procedure uses two original samples to calculate a new sample, which takes place on a straight line connecting the initial samples. The impulse and frequency response of the interpolator filter (IF) are depicted in Fig. 5a and 5b, respectively. One may observe that the IF impulse response ($IF\,[n]$) is triangular shaped, and the interpolator filter frequency response (IFFR) is similar to those of low-pass filters, limited to the factor L. Thus, the IF impulse response is defined in (13), being composed by $2 \cdot L + 1$ coefficients.

$$IF\,[n] = \begin{cases} 1 - {}^{|n|}/_{L}, & |n| \leq L \\ 0, \text{otherwise} \end{cases}\ . \quad (13)$$

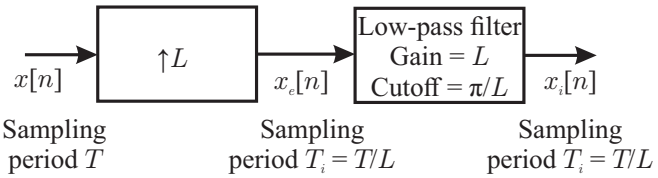

Fig. 4: Upsampling system [10].

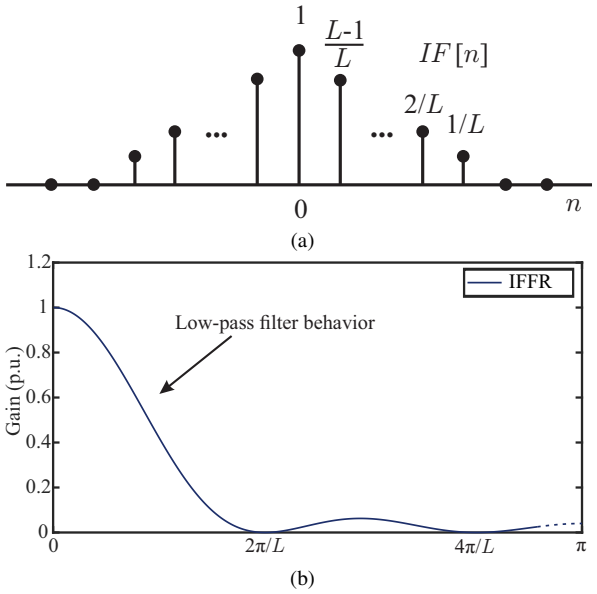

Fig. 5: Interpolator filter: (a) Impulse response; (b) Frequency response.

IV. Proposed Scheme

In this paper, the linear interpolation technique is proposed for DFRs with relatively low sampling rates. Here, case studies are carried out considering DFRs which employ 1,024 samples per cycle. Thus, the number of samples in the records are increased to obtain the same number of samples found in traditional TW-based fault locators. By doing so, although only the inferior transient spectrum band is available, as reported in [7], TW filters can be adapted to properly analyze such a spectrum content, preserving accuracy in the TW arrival time stamping procedure.

A. Analyzed TW Filter

The analyzed TW filter is proposed in [4] for TW applications on transmission lines. It has been successfully used in TWFL methods, such that it is adopted here to be applied in conjunction with the proposed interpolation-based solution. In this work, the DS filter implementation is in accordance to [12], whose frequency response is depicted in Fig. 6, where the DS filter model is validated through comparisons with the original one built into a commercial available time-domain-based relay [6]. Moreover, besides the proposed scheme, the DS filter is also used to implement the classical TW1-method, considering the number of coefficients (NDS) reported in [6], but without applying interpolation procedures to simulated data.

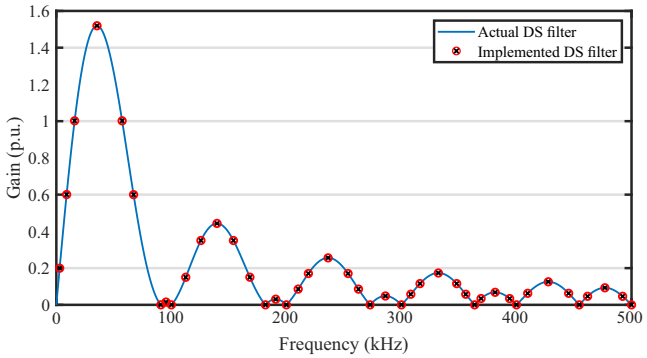

Fig. 6: DS filter frequency response validation [6].

B. Anti-Aliasing Filter

The parameters of the analog Butterworth filters used to assess the fault location solutions are presented in Table I. Aiming to define the IF and DS filter settings, a series of studies were also performed.

TABLE I: Analog Butterworth filter settings for the evaluated methods.

Method	Order	fc (Hz)	Method	Order	fc (Hz)
PH1	3	180	PH2	3	180
TW1	2	400 k	Proposed	2	24,576

C. Proposed Combination of IF and DS Filter

Combinations of different values of L and number of coefficients of the DS filter (NDS) were analyzed. Figs. 7a and 7b present the frequency responses obtained from the convolution of implemented anti-aliasing Butterworth filters, DS filters, and IF filters, considering all the analyzed combinations between L and NDS. From the obtained results, $L = 16$ is chosen because the interpolated frequency of 983,040 Hz is the closest one to the 1 MHz sampling frequency used in the actual TW-based device taken as reference [6]. Moreover, the original DS filter with NDS $= 21$ reported in [6] results in step responses with unitary gains when applied to signals sampled directly on 1 MHz. However, here, NDS $= 251$ is chosen to provide a step response with gain close to the unit for the combination of DS, IF, and Butterworth filters when applied to the interpolated signal using $L = 16$ (see Fig. 8). By doing so, the proper analysis of the lower frequency spectrum band, which concentrates most of line fault-induced transients energy, is guaranteed [7]. It is noteworthy that the inherent delay on TW peak detection when using the DS Filter with NDS $= 251$ does not compromise the fault location procedure, since the same filter is applied to signals from both line terminals, thereby the time difference between incident local and remote TWs is preserved, as discussed in Sec. VII.

V. Evaluated Power System

The test power system used to validate the proposed interpolation-based solution was modeled in ATP/ATPDraw and it corresponds to part of the 500 kV/60 Hz Brazilian

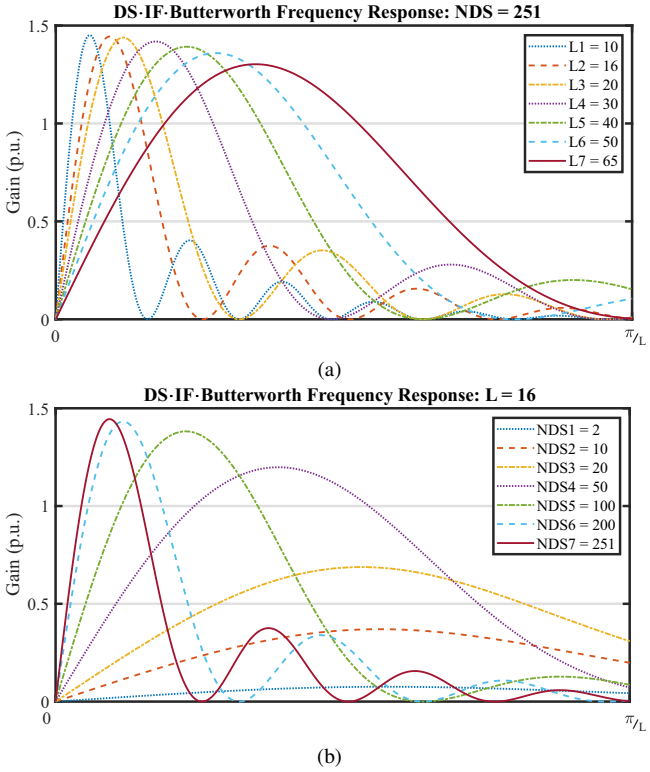

Fig. 7: Convolution of Butterworth, DS, and IF filters in function of: (a) L; (b) NDS.

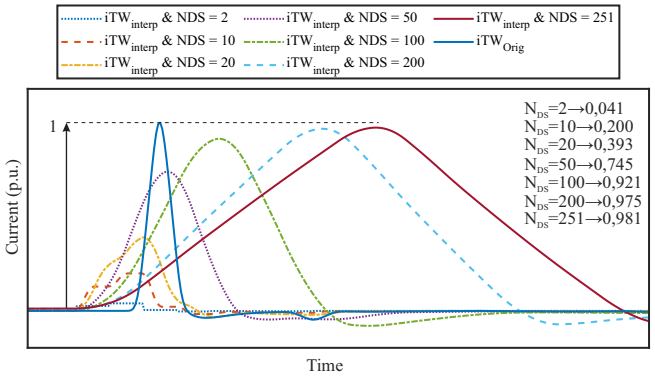

Fig. 8: Comparison between the DS filter step response using the signal sampled directly on 1 MHz and the interpolated one obtained from the signal sampled on 61.44 kHz.

interconnected power system described in Fig. 9. Through the 500 kV lines, two Brazilian states are interconnected to the rest of the Brazilian power grid. Between power stations Lechuga and Xingu there are 1,173 kilometers of 500 kV overhead transmission lines which cross the Amazon rainforest, as depicted in Fig. 10, facing a high density of trees that achieve from 40 meters up to 110 meters in height. It highlights the importance of using an accurate fault location method for this kind of line.

Besides the environmental challenging, the following equipment are installed nearby, revealing how much complex is to operate such a part of the Brazilian power grid:

(i) 800 kV bipole LCC-HVDC 2,084 km long between

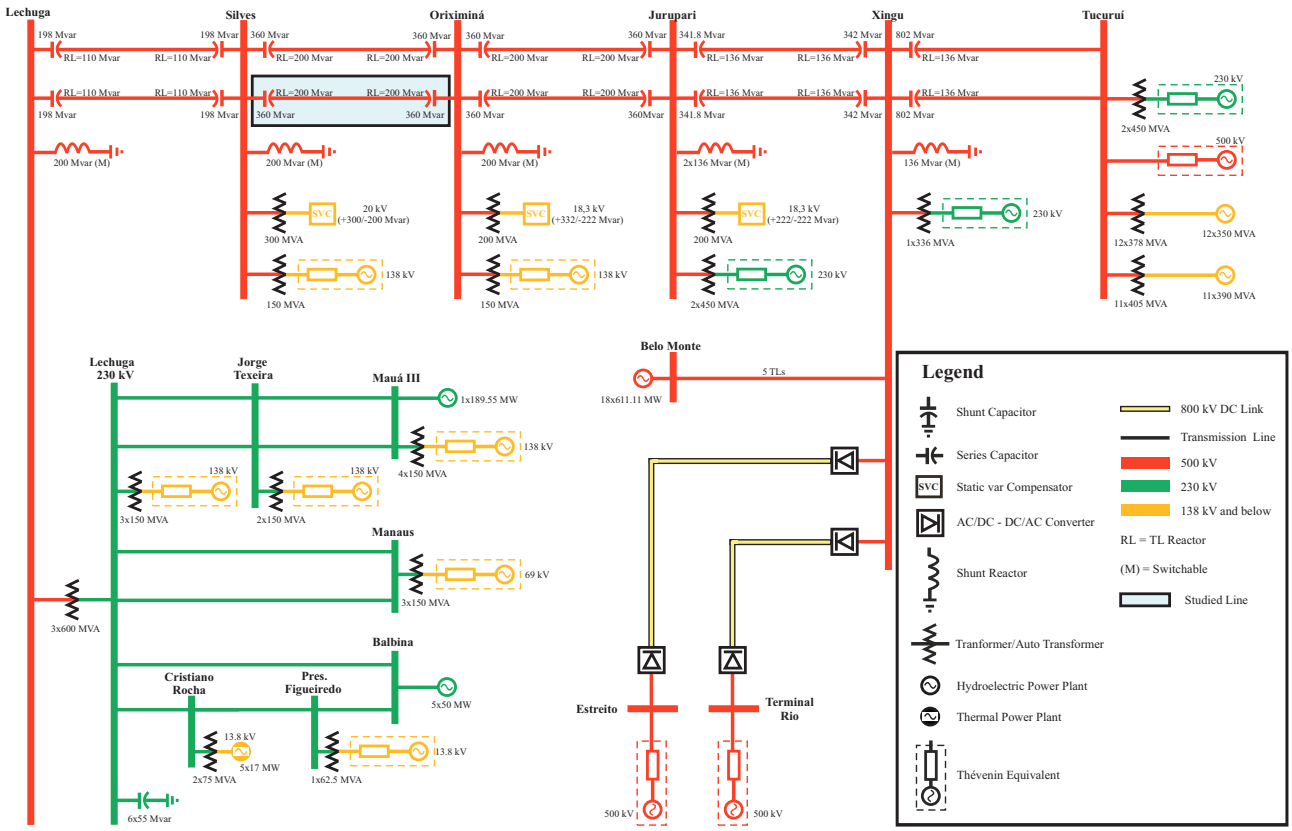

Fig. 9: Single-line diagram of the part of the Brazilian power grid modeled in ATP/ATPDraw.

Fig. 10: Photograph of the evaluated 500 kV double-circuit transmission line between stations Silves and Oriximiná.

stations Xingu and Estreito;

(ii) 800 kV bipole LCC-HVDC 2,518 km long between stations Xingu and Terminal Rio;

(iii) Three 500 kV SVCs installed on stations Silves, Oriximiná, and Jurupari;

(iv) FSCs on each terminal of the double-circuit line between stations Lechuga and Xingu, and on the terminal Xingu of the double-circuit line between Xingu and Tucuruí;

(v) Belo Monte hydroelectric power plant with 18 generator units whose capacity is 611 MW each;

(vi) Tucuruí hydroelectric power plant with 23 generator units, among which 12 have capacity of 350 MW each, whereas 11 have capacity of 390 MW each;

(vii) Thermal and hydroelectric power plants on the 230/138 kV subsystems connected to the Lechuga station.

VI. Simulations Description

Aiming to properly explain the methodology used to evaluate the algorithms investigated in this paper, it is essential to understand the applied signal processing procedures, which are summarized in Fig. 11. From the figure, one observes that:

1) For PH1 and PH2 methods, the Fourier full cycle filters were applied to estimate voltage and current phasors from the monitored signals, considering a sampling frequency of 960 Hz, as described in Fig. 11a. These phasors are then used as inputs of PHFL methods;
2) High sampling frequency current signals sampled at 1 MHz are used as inputs of both DS filter and modal transforms applied to obtain aerial mode TWs in TW1-method, as shown in Fig. 11b;
3) As depicted in Fig. 11c, the proposed IF is applied to the low sampling frequency data to expand the original sampling frequency 66.44 kHz (i.e., 1,024 samples per cycle) to the value closest to 1 MHz.

Table II represent a description of simulations carried out to evaluate and validate the proposed solution, where 132 phase-A-to-ground (AG) and 132 phase-B-to-phase-C (BC) fault cases were simulated on the circuit 2 of the 500 kV double-circuit line between stations Silves and Oroximiná

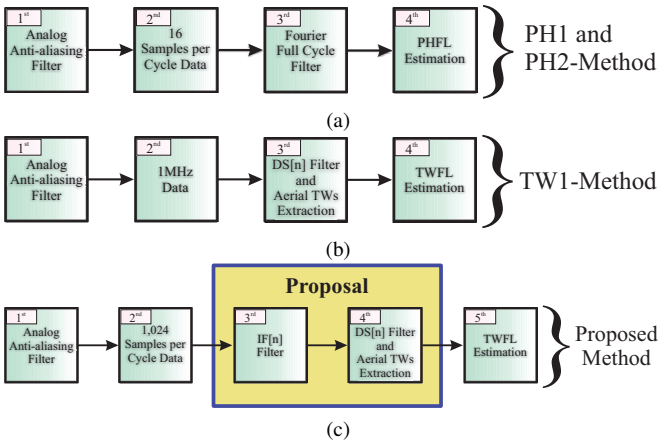

Fig. 11: Signals processing for: (a) PH1 and PH2-methods; (b) Traditional TWFL; (c) Proposed interpolation application.

(with 333.5 km long and $\tau = 1.116$ ms), varying the fault distance from station Silves. Two loading scenarios were considered: 1) light load (with 360 A at steady-state); and 2) heavy load (with 805 A at steady-state). For each loading condition, 66 cases were simulated, resulting in the above-mentioned 132 cases per fault type, accounting for 264 case studies. Furthermore, all scenarios were simulated as solid faults, i.e., fault resistance was set with values equal to 1E-5 Ω. By doing so, solid faults could be simulated. Finally, it is also worth mentinoing that the power system simulation were carried out with a frequency equal to 1 MHz to emulate more realistic scenarios and associated phenomena. Therefore, the assessed algorithms are applied to simulated fault records with a sampling frequency equal to 960 Hz for the PH1 and PH2-methods, 61.44 kHz for the proposed method, and 1 MHz for the TW1-method.

It is important to emphasize that the studied double-circuit 500 kV transmission line between stations Lechuga and Oroximiná was modeled using J. Marti model, being the SVC models connected at the stations Lechuga, Silves and Oroximiná, such as indicated by the manufacturer. The FSCs were modeled to provide the expected behavior of the internal protections and phenomena associated to its triggering and, to represent the HVDC lines, the models of 800 kV Xingu / Estreito and Xingu / Terminal Rio links were also included in the ATP/ATPDraw simulation.

TABLE II: Details of simulated cases.

Parameter	Value
Power system simulation frequency	1 MHz
TW1 method sampling frequency	1 MHz
PH1 and PH2 methods sampling frequency	960 Hz
Proposed method input sampling frequency	61.44 kHz
Fault resistance	1E-5 Ω
Number of fault locations	66
Steady-state loading scenarios	2 (360 A and 805 A)
Fault types	2 (AG and BC)

VII. Results and Discussion

This section describes the performance analysis of the assessed algorithms, but firstly the PHFL-based algorithms issues are highlighted and the differences between TWs waveforms obtained with TW1 method and the proposed one are presented. Then, the comparison of PH1, PH2, TW1, and proposed methods are carried out over the 264 simulated cases.

A. Waveforms Analysis

In order to further explain the performance of each fault location method, consider Fig. 12 which depicts the current signals measured at station Silves for an AG solid fault with inception angle equal to 90° simulated at 25 km (i.e., 0.075 pu of the line length) from Silves in the circuit 2 of the 500 kV double-circuit line between stations Silves and Oriximiná. The fault location estimations m obtained from both PH1 and PH2, and the TW1 and proposed method were calculated from these waveforms.

From Fig. 12a, during the pre-fault period, one can observe harmonic distortions even in the steady-state currents generated by the natural behavior of thyristors switching in SVCs and HVDCs. The pre-fault period ends with the arrival of the first incident TWs, followed by the phase-A amplitude-raising. The monitored line and the others in its vicinity are series compensated, so that subsynchronous oscillation may take place during faults [13]. Thus, even when the FSC spark gap is triggered in the station Silves, the subsynchronous oscillation phenomena remains. The FSC bypass at Silves also induces additional transients, which may affect fault location methods. Moreover, it can be noticed that the subsynchronous oscillation leads m estimation to present errors when PHFL-based methods are used. This effect is depicted in Fig. 12b. Indeed, when fault transients reach Silves, the m values estimated by PH1 and PH2 methods oscillate around the actual fault location. It can be also observed that the PH2 presents a better performance than the PH1, but their performances are compromised by the subsynchronous oscillation.

Figs. 12c and 12d depict the aerial mode current waveforms ($i\alpha TW$) computed for signals measured at stations Silves and Oriximiná, which are used by TW1 and proposed method. One can see that the subsynchronous oscillation phenomena and SVC and HVDC effects over steady-state do not affect TW-based solutions, because the first incident TWs on both terminals can be easily identified from the waveforms analysis.

Additionally, one can see that, despite the difference between the input sampling frequencies for TW1 and proposed method as presented in Table II, the obtained result when subtracting NL by NR (0.95 ms and 0.947 ms) for both methods is quite accurate, leading to fault locations of 25.2516 km and 24.7863 km, respectively. Indeed, the use of a DS filter with NDS $= 251$ in the proposed method does not jeopardize the first incident TW detection. Also, a lower attenuation is observed in the $i\alpha TWR$ in the proposed technique in comparison with the TW1 method, which shall be better investigated in future works to investigate the feasibility of precise single-ended TWFL solutions using low sampling rate interpolated signals.

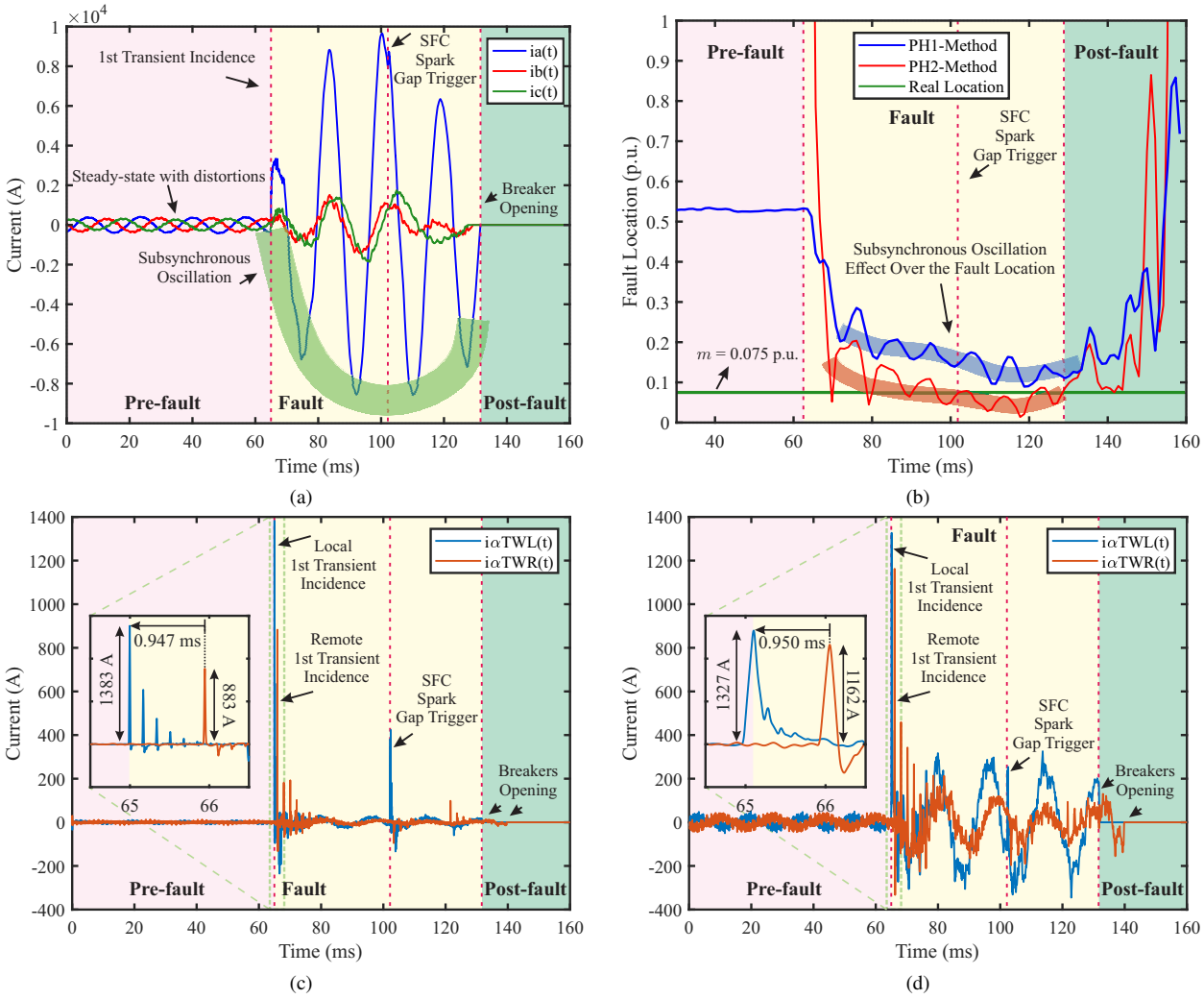

Fig. 12: PHFL and TWFL-methods behavior: (a) Monitored current signals; (b) PH1 and PH2-methods; (c) TW1 method; (d) Proposed method.

B. Fault Location Algorithms Comparison

As the main result, a comparison between the fault location errors for the evaluated algorithms in each fault scenario is depicted in Fig. 13. It can be seen that for the assessed AG faults, the influence of SVCs, HVDCs, and subsynchronous oscillation caused by FSC jeopardizes PH1 and PH2-methods, resulting in errors about few tens of kilometers. Although the PH1 method also presents approximately the same error rates for BC fault cases, the PH2 method has an enhanced accuracy. Conversely, TW-based methods TW1 and the proposed one are not jeopardized by the fault type, load scenario, and different equipment installed on the system, because they do not influence the TWs generated at the fault point. As a result, high accuracy is guaranteed for both methods, highlighting the reliability and robustness of TWFL approaches.

Furthermore, although the proposed method results in average fault location error in the order of 500 meters (using low sampling rate interpolated signals), these errors are still about only 350 meters greater than those obtained via traditional TW1-method (using high sampling rate signals). Even so, these errors are considered quite close to each other, such that benefits of the proposed solution can be clearly identified, especially from a cost perspective, since it is much cheaper to develop a device with 61.44 kHz sampling frequency rather than with 1 MHz. Indeed, the obtained errors remain around 0.15% of the line length, and they are almost constant for faults at different points on the line. Therefore, the obtained results highlight the effectiveness of the proposed interpolation methodology for TW-based applications when DFRs with high sampling rates are unavailable.

VIII. Conclusions

This paper proposes the use of an interpolation technique in conjunction with DS filter and TW-based fault location approaches, when DFRs with high sampling rates are unavailable. As a result, relatively low sampling rates can be used. Moreover, the proposed method presents an almost unitary step response, providing good representation of arriving TWs at line terminals. An amount of 264 case studies were carried out, allowing the comparison of the proposed methodology with other phasor-based techniques and the traditional TW-based double-ended solution. To do

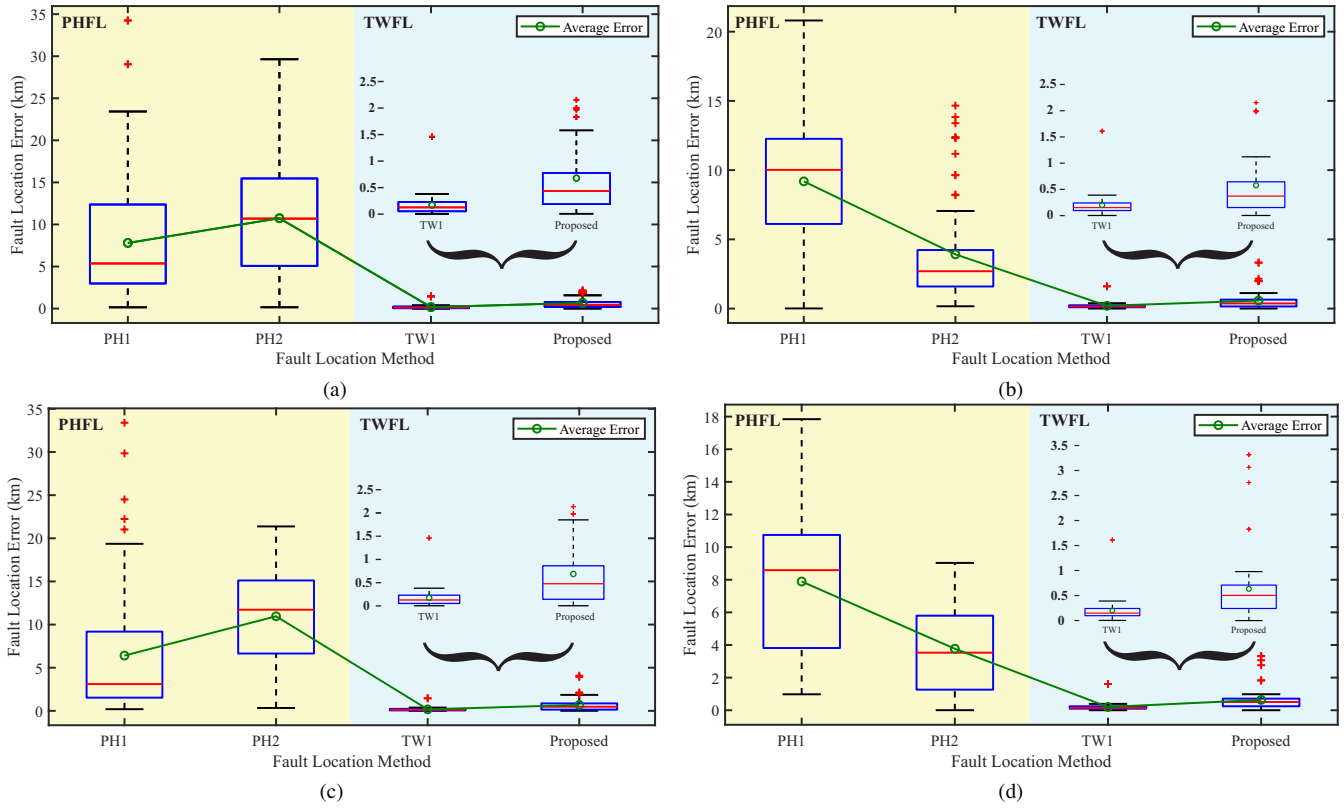

Fig. 13: Fault location algorithms comparison: (a) A-phase-to-ground on the light load scenario; (b) B-phase-to-C-phase on the light load scenario; (c) A-phase-to-ground on the heavy load scenario; and (d) B-phase-to-C-phase on the heavy load scenario.

so, ATP/ATPDraw simulations of faults on a 500 kV/60 Hz Brazilian transmission system were performed.

In the simulations, PHFL-based and TWFL-based methods are described and assessed through waveforms. The obtained results show that the proposed solution is effective, being capable of estimating faults with an accuracy comparable to those obtained via traditional TW-based fault location methods, but using a much smaller sampling rate, which is attractive from a cost perspective. Indeed, for the four evaluated scenarios, the average errors remain in the order of 500 m, attesting to the validity of the proposed solution.

IX. Acknowledgment

This work was developed in partnership with IATI and CEPEL within the scope of the R&D project PD-06908-0003/2021, sponsored by the Brazilian Agency of Electrical Energy (ANEEL) and EVOLTZ. The authors thank the cooperation of Ms. Larissa Silva (EVOLTZ) and Dr. Marco Antonio M. Rodrigues (CEPEL).

References

[1] A. Johns and S. Jamali, "Accurate fault location technique for power transmission lines," in *IEE Proceedings C (Generation, Transmission and Distribution)*, vol. 137, no. 6. IET, 1990, pp. 395–402.

[2] P. Gale, P. Crossley, X. Bingyin, G. Yaozhong, B. Cory, and J. Barker, "Fault location based on travelling waves," in *IET Fifth International Conf. on Developments in Power System Protection*, 1993, pp. 54–59.

[3] A. C. Report, "Bibliography and summary of fault location methods [includes discussion]," *Transactions of the American Institute of Electrical Engineers. Part III: Power Apparatus and Systems*, vol. 74, no. 3, pp. 1423–1428, 1955.

[4] E. Schweitzer, A. Guzmán, M. Mynam, V. Skendzic, B. Kasztenny, and S. Marx, "Locating faults by the traveling waves they launch," in *67th IEEE annual conference for protective relay engineers*, 2014, pp. 95–110.

[5] T. P. S. Bains, T. S. Sidhu, Z. Xu, I. Voloh, and M. R. D. Zadeh, "Impedance-based fault location algorithm for ground faults in series-capacitor-compensated transmission lines," *IEEE transactions on power delivery*, vol. 33, no. 1, pp. 189–199, 2017.

[6] *Ultra-High-Speed Transmission Line Relay Traveling-Wave Fault Locator High-Resolution Event Recorder*, Schweitzer Engineering Laboratories, 2019. [Online]. Available: https://selinc.com/products/T400L/

[7] F. V. Lopes, R. Reis, D. Facina, K. Melo, K. Dantas, and F. Costa, "How much "villain" is the anti-aliasing filter for traveling wave-based fault location methods?" *Electric Power Systems Research*, vol. 212, p. 108369, 2022.

[8] *Exmpertmeter EM920 High Performance Revenue Socket Meter Cutting Edge Power Quality Analyzer Fast Transient and Fault Recorder*, SATEC Ltd., 2017. [Online]. Available: https://www.satec-global.com/EM920/

[9] *G5DFR Multi-Functional Digital Fault Recorder*, Elspec Engineering Ltd., 2018. [Online]. Available: https://www.elspec-ltd.com/metering-protection/g5-multi-functional-digital-fault-recorder/

[10] A. V. Oppenheim, *Discrete-time signal processing*. Pearson Education India, 1999.

[11] R. E. Crochiere and L. R. Rabiner, "Multirate digital signal processing: Prentice-hall, inc. englewood cliffs, new jersey 07362, 1983, 411 pp., isbn 0-13-605162-6," 1983.

[12] E. P. A. Ribeiro, F. V. Lopes, J. P. G. Ribeiro, and E. J. Leite, "Atp/models differentiator-smoother filter model validated using actual time-domain relay," in *2018 Workshop on Communication Networks and Power Systems (WCNPS)*. IEEE, 2018, pp. 1–4.

[13] P. M. Anderson and R. G. Farmer, *Series compensation of power systems*, 1996.